Multiple Emission from Sulfur Complexes of Rhodium(III) and Iridium(III)

James T. Merrill† and M. Keith DeArmond*

Contribution from the Department of Chemistry, North Carolina State University, Raleigh, North Carolina 27650. *Received August 3, 1978*

Abstract: The preparation, purification, absorption, and emission spectra and emission lifetimes are reported for four trisdithioketone complexes of rhodium(III) and iridium(III). The broad, structureless, red emission observed for the four complexes overlaps with the absorption spectra and can for each compound be resolved into two Gaussian components. Decay curves measured at the emission peak wavelength can be fit with a sum of two exponentials. The photoselection technique is used to verify the two-state emission from these complexes. Analysis of these data indicates that the multiple emission is an intramolecular phenomena with the two emitting states assigned as a d-d and a charge transfer (Π-d*). Excitation spectra indicate the existence of independent pathways of population for the two states. Temperature-dependent lifetimes and quantum yields permit measurement of activation energies in plastic solvent media. Kinetic models are presented and decay data interpreted as indicating the presence of a finite rise time for the emission of one of the excited states.

Introduction

The relaxation of excited states in transition-metal complexes is generally determined by (1) the radiative-nonradiative competition and (2) the pathway (spin forbidden or spin allowed) of the relaxation. The experimental data used to delineate the competition and the pathway have been primarily of three types: emission and absorption spectra, decay times, and quantum yields.

Among the first series transition metal ions, the d^3 ion chromium is the only species exhibiting luminescence in a large number of complexes, thereby providing sufficient structural variation to enable systematic comparison of the three types of data. To summarize, the data compiled for Cr^{3+} complexes indicate that at 77 K phosphorescence from the ^2E is the usual emission pathway, and that the quantum yields are small owing to efficient nonradiative relaxation both from the emitting ^2E and from the photoactive $^4T_2$ state. These results are well summarized in the reviews of Forster[1,2] and Fleischauer[3] and the work of Robbins and Thomson.[4]

The luminescent heavy transition metal d^6 complexes of Ru^{2+}, Os^{2+}, Rh^{3+}, and Ir^{3+} also afford a sufficient number of complexes to provide the necessary structural perturbation to elaborate the pathway and the radiative-nonradiative competition.

Since the large crystal field splitting of heavy transition metal complexes permits substantial variation of the orbital character of the emitting and higher states, a variety of relaxation pathways may occur dependent upon the coupling between these lowest states.[5,6] For example, "localized orbital" (d-d) emission is observed for many complexes having a crystal field state lowest in energy (i.e., $[Rh(bpy)_2Cl_2]^+$ where bpy = 2,2′-bipyridine) while a "delocalized orbital" emission (charge transfer (d-Π*) or ligand localized (Π-Π*) transition) can be observed for a number of d^6 complexes similar in structure (as $[Rh(bpy)_3^{3+}]$).[7] Additionally, the extended d shell radius of the heavy-atom species and the higher energy of the d subshell affords the possibility of extensive mixing of the d and Π type ligand orbitals, although no certain example of such a mixed orbital emission has yet been found. Therefore, the rapid and isotropic vibrational deactivation of excited electronic states with consequent equilibration of energy to all portions of the chromophore as observed for most large organic molecules may not always occur for the relaxation of large inorganic chromophores. For example, variation of luminescence quantum yield with wavelength of excitation[7] has been verified by measurement[8] of rise and decay times for the $[Rh(bpy)_2Cl_2]^+$. More significant is the observation of multiple emitting states for the mixed ligand complexes[9] $[Rh(bpy)_2phen]^{3+}$ and $[Rh(phen)_2bpy]^{3+}$ and subsequently for mixed ligand complexes of formula $[Ir(LL')Cl_2^+]$ where L and L′ are different diimine ligands.[10,11] The former Rh^{3+} emission has been interpreted as due to a localized exciton (single ring) emission while the Ir^{3+} emission has been interpreted as originating from states of different orbital origin (i.e., Π-Π* and d-Π* transitions). Most recently two additional cases of multiple emission from heavy metal transition metal systems have been presented and these interpreted as originating from states of different orbital origin.[12,13] Although the various interpretations of some of these multiple emissions may ultimately be altered, the central fact is that coupling between states of different orbital or different spatial origin is apparently not complete, i.e., not isotropic. Consequently different relaxation channels can occur dependent upon the state initially excited.

In all but one of the previous reports of multiple emission, the complexes have involved diimine ligands. The generality of this multiple emission phenomena can only be determined by examination of additional heavy metal complexes in which, as in the diimine complexes, the zeroth-order energy levels of the d-d and ligand Π-Π* transition are expected to be of comparable energy. The β-diketone ligands acetylacetone (acac), trifluoroacetylacetone (tfacac), and hexafluoroacetylacetone (hfacac) produce complexes with a low energy ligand Π-Π* system. Examination of the crystal field parameters provided by the absorption and emission spectra[14,15] of the $Rh(dtp)_3$ and $Rh(dtc)_3$ complexes (where dtp = dithiophosphate and dtc = diethyldithiocarbamate) suggests that the sulfur analogues of the β-diketone Rh(III) and Ir(III) complexes might provide the appropriate combination of electronic factors to generate luminescent systems with either (a) substantial interaction of d and Π ligand orbitals or (b) close lying localized (d-d) and delocalized (Π-Π* or charge transfer) lowest excited states.

In an ideal case where appropriate dilute single crystal samples could be obtained, absolute absorption and emission polarization data can be useful in assigning the orbital origins of absorption and emission transitions. At present such a single-crystal technique is not possible for these sulfur chelate systems. However, the emission photoselection technique introduced by Weigert[16] and subsequently developed by others[17-21] has significant advantage for determination of the relative orientation of emission and absorption oscillators for randomly oriented samples.

† Chemistry Department, University of Houston, Houston, Texas.

0002-7863/79/1501-2045$01.00/0

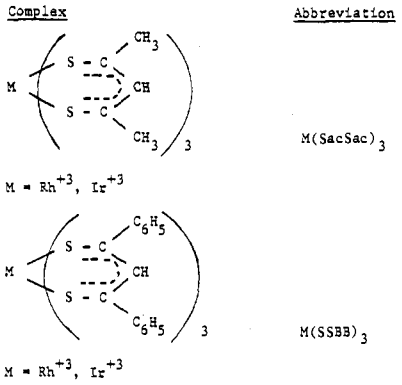

Figure 1. Formulas and abbreviations of chelates.

El-Sayed[22,23] made extensive use of the photoselection technique to determine nonradiative selection rules for aromatics possessing low-lying $\Pi-\Pi^*$ and $n-\Pi^*$ type states. In addition, El-Sayed[24,25] has defined the spin-orbit mechanism for aromatics containing heavy halogen atoms. Lim and coworkers[26-28] have utilized the method to determine the vibronic perturbation of the emitting triplet in aromatic ketones and to assign the multiple emission of 1-indanone. To date, a single published example of the photoselection technique exists for inorganic materials, this for the $[Ru(bpy)_3^{2+}]$ complex.[29]

Therefore, the photoselection technique has been used here to attempt to verify the two-state emission from these sulfur chelates. The polarization is defined as

$$P = \frac{I_{vv} - I_{vh}}{I_{vv} + I_{vh}} \quad (1)$$

where I_{vv} and I_{vh} are the measured emission intensities with the analyzers vertical (v) and horizontal (h), respectively. The excitation source is polarized vertical (v).

Since the accidental overlap of two emitting states implies parallel relaxation pathways with a lack of communication between the pathways, delineation of these pathways requires additional data. Therefore, in addition to polarization spectra, relative quantum yields as a function of wavelength of excitation (excitation spectra) and temperature-dependent emission data have been accumulated to attempt to elaborate the relaxation of the excited states.

Ultimately answers to the following questions are necessary: (1) Why do the emitting states not communicate? (a) Electronic (orbital) origin factors? (b) Vibrational factors? (c) Combination of electronic and vibrational? (2) Does "communication" have an energy dependence? Therefore, this paper is the report of the preparation, purification, and spectroscopy for the neutral sulfur chelate complexes $Rh(SacSac)_3$, $Ir(SacSac)_3$, $Rh(SSBB)_3$, and $Ir(SSBB)_3$ (where SacSac = dithioacetylacetone and SSBB = dithiodibenzoylmethane, Figure 1).

Experimental Section

Solvents. Low-temperature absorption and emission spectra were obtained in ETA (diethyl ether–toluene–ethanol, in respective parts of 1:2:1), methylcyclohexane, and poly(methyl methacrylate) (PMM).

Ethanol was purified by the method of Halper[30] and diethyl ether by the method of Fieser and Fieser.[31] Toluene was stirred with concentrated sulfuric acid until the acid was colorless, washed three times with water, dried over anhydrous calcium sulfate, and fractionally distilled onto molecular sieves. Eastman "Spectro" decalin and Phillips "99 mol % pure" methylcyclohexane were used without further purification. Poly(methyl methacrylate) (PMM) was dissolved in ethyl acetate and an equal volume of cyclohexane was added to precipitate the PMM. The PMM was filtered, washed with ether, and air dried. Polymer samples were obtained by standard techniques.

Synthesis. The SacSac complexes of rhodium and iridium were prepared by the method of Heath and Martin[32,33] with yields of less than 3.0 and 0.5%, respectively. The $Ir(SacSac)_3$ was purified by passage through a silica gel column (2.5 × 45 cm), eluted with benzene and recrystallized from a chloroform–ethanol mixture. The $Rh(SacSac)_3$ was purified by preparative thin layer chromatography (silica gel) with a toluene eluent, with subsequent recrystallization from petroleum ether.

The infrared and ^1H NMR spectra were consistent with the reported spectra[32] and no carbonyl stretching bands were observed.

All elemental analyses were performed by Atlantic Microlab Inc., Atlanta, Ga. Anal. Calcd for $Rh(SacSac)_3(C_{15}H_{21}S_6Rh)$: C, 36.27; H, 4.26; S, 38.73. Found: C, 36.14; H, 4.27; S, 38.59. Calcd for $Ir(SacSac)_3$: C, 30.75; H, 3.61; S, 32.83. Found: C, 30.94; H, 3.50; S, 32.71.

Attempts to synthesize the $Rh(SSBB)_3$ complex in a manner analogous to the SacSac synthesis were unsuccessful; therefore the following reaction sequence utilizing a stable free radical ligand[34] material was developed.

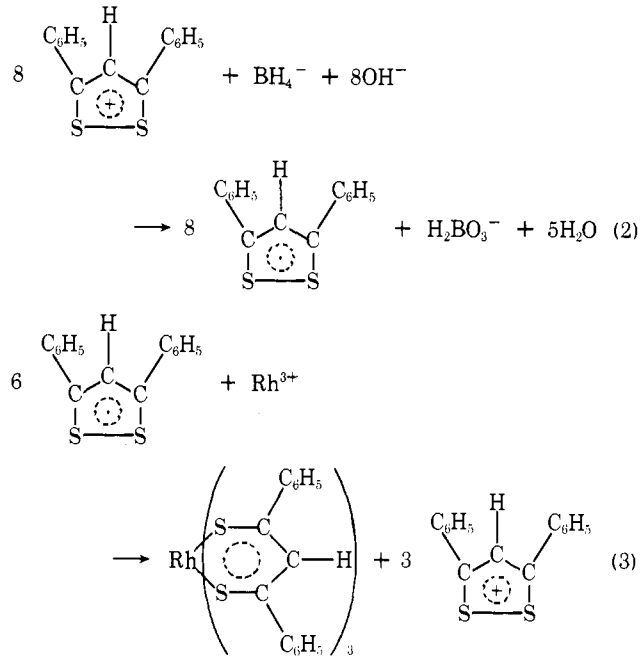

The 3,5-diphenyldithiolium chloride was prepared by the modified method of Beckgaard, Parker, and Pedersen[34] and recrystallized from 95% ethanol. The metal complex syntheses were carried out in deaerated solvents and performed in a nitrogen-filled glovebag.

Preparation of $Rh(SSBB)_3$. 3,5-Diphenyl-1,2-dithiolium chloride (7.5 g) was suspended in ethanol and sodium borohydride (1 g) added. Excess sodium borohydride was destroyed with a solution of hydrogen chloride dissolved in ethanol. Commercial rhodium trichloride hydrate (1.01 g) in 50 mL of deionized water was added dropwise to the free-radical solution. The mixture was refluxed for 2 h, then left at room temperature overnight. The crude product washed with hot water, hot ethanol, and ether was dissolved in benzene and eluted with benzene from an alumina column. The first colored fraction yielded a deep violet colored product (35% yield) that recrystallized from an ethanol–chloroform mixture dissolution. The $Rh(SSBB)_3$ material was checked exhaustively by thin layer chromatography with ~50 different combinations of plate (silica and alumina checked with a variety of solvents). Only a single spot was detectable for all combinations.

Preparation of $Ir(SSBB)_3$. The Ir complex was prepared by analogy to the Rh complex with these differences. The mixture was refluxed for 16 h. Chloroform solvent was used for the alumina chromatography with a 2/1 v/v mixture of benzene–chloroform used as the eluent. The final recrystallization from an ethanol–benzene solution yielded 0.050 g of the product (1.3% yield). Anal. Calcd for $C_{45}H_{33}S_6Ir$: C, 56.40; H, 3.47; S, 20.07. Found: C, 56.71; H, 3.60; S, 20.01.

Spectral Measurements. Absorption measurements were obtained on a Cary 14 spectrometer. Measurements at 83 K were made in a copper block cryostat.

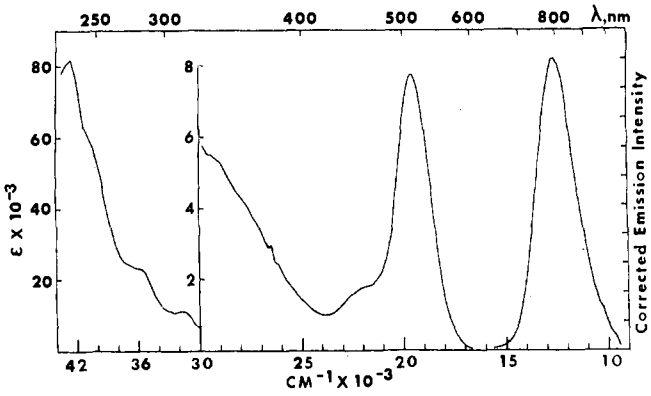

Figure 2. Low-temperature absorption and emission of $Rh(SacSac)_3$.

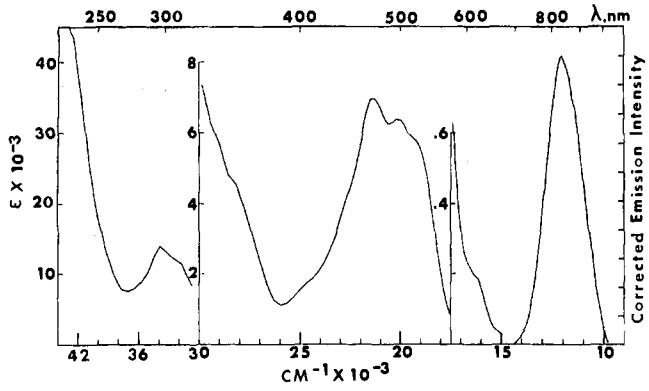

Figure 3. Low-temperature absorption and emission of $Ir(SacSac)_3$.

Emission spectra for the solutions of ETA solvent were taken with an Aminco-Bowman spectrofluorometer at 77 K with an Aminco-Kiers phosphoroscope. A grating blazed with maximum efficiency at 750 nm was installed in the emission monochromator and a cooled RCA 7102 photomultiplier tube was used to detect the emitted light. Excitation wavelengths used were 313 and 365 nm. Decay measurements were done with a Laser Energy Inc. pulsed N_2 laser excitation with the monochromatic pm tube signal determined from the oscilloscope display or from the recorder output of a PAR Model 162/164 boxcar integrator.

Corrected excitation spectra measurements were made with two different techniques. The first technique employed the Aminco-Bowman spectrofluorometer with excitation from a 200-W Xe lamp. Intensities were corrected by two methods (A and B). Method A[35,36] was used in the wavelength region from 500 to 700 nm. Light from the excitation monochromator was reflected from a solid block of $MgCO_3$ onto the entrance slit of the emission monochromator. The emission monochromator wavelength dial was adjusted for maximum deflection of the output recorder and the intensity at that wavelength recorded. This process was repeated at 5-nm intervals. A calibrated quartz-halogen lamp manufactured by Electron Optics Associates was positioned above the sample compartment and its spectrum recorded. Method B,[37] used for the region 370–600 nm, employed a 8 g/L solution of Rhodamine B in ethylene glycol as a quantum counter with the emitted light viewed at 90° to the excitation beam. Since small-diameter sample tubes were used, geometry effects should be minor with 90° observation. This was confirmed by also viewing the emission of the quantum counter at 180° with appropriate filters.

The second technique utilized a 0.25-m Jarrell-Ash monochromator and broad band detection (filter isolated) of the emitted light. The exciting light was modulated at 90 Hz with a Princeton Applied Research Corp. (PAR) 125 light chopper. The photomultiplier output was amplified by a PAR Model HR-8 lock-in amplifier. The relative intensity of the exciting light was measured with the Rhodamine B quantum counter.

The apparent excitation spectra were corrected by dividing the recorded sample output at each wavelength by a correction factor. With the Rhodamine B quantum counter, the correction factor is just the recorded quantum counter output at the appropriate excitation wavelength. The correction factor for the quartz-halogen lamp method was calculated by the equation

$$\text{correction factor} = \frac{R}{E\lambda} \tag{4}$$

where R is the recorded output of the calibrated lamp, λ is the excitation wavelength, and E is the true spectrum output of the lamp in units of $\mu W/cm^2 \cdot s \cdot nm$.

Photoselection Measurements. All photoselection experiments were run on the Aminco-Bowman spectrofluorimeter equipped with Glan-Thompson polarizing prisms. The reduced emission intensity necessitated a specially fabricated photomultiplier housing adapter to allow insertion of the PAR Model 125 light chopper for lock-in amplification of the pm output.

Variable Temperature Measurements. All variable temperature measurements were performed with an emission spectrophotometer assembled in these laboratories with two 0.25-m monochromators manufactured by Jarrell-Ash. This instrument, utilizing a 450-W xenon or 1000-W mercury-xenon lamp, permitted greater sensitivity and more flexibility with the sample compartment. Slit widths were 0.5 mm for the relative intensity measurements and 1.0 mm for the lifetime measurements.

For recording emission and excitation spectra the lamp output is modulated with a PAR Model 125 light chopper and the emission signal detected with a PAR Model HR-8 lock-in amplifier (a phase- and frequency-sensitive amplifier).

For recording time dependent data the photomultiplier output is signal averaged and amplified by a PAR Model 162/164 boxcar averager. Short duration, 10 ns, pulses from a Laser Energy Inc. pulsed N_2 laser excite the sample. Because the intensity of these pulses varies ±10–20%, a small fraction of the intensity is diverted by a quartz plate beam splitter to excite a reference compound (Optical Integrator, OI). The signal from the OI-photomultiplier is also fed to the boxcar averager. With the ratio option, A/B, A = analytic signal, B = reference signal, the A channel is scanned with respect to time (t = 0 is the nearly instantaneous pulse of exciting light) and the B channel is held at a constant time.

Signal intensities were increased by a factor of 3–6 by placing the optical window of the Aminco-Kiers Dewar into the center of a specially fabricated hemispherical aluminum reflector.

A variable temperature glass cryostat using boiling N_2 has been constructed for use with the spectrophotometer. The heater circuit from a JEOL (Japan Electron Optics Co.) Model JES-VT-3 temperature controller with the JEOL supplied Dewar and heater was used to regulate the temperature of the cryostat. The sample temperature was equilibrated for approximately 5 min, a measurement (lifetime or intensity) made, and then the temperature increased 7–15 K. This procedure was repeated until the measured temperature was approximately 273 K or the maximum intensity was 5% of that at 77 K.

Relative emission intensities were determined with the filter-isolated 365-nm output of a 1000-W Hg–Xe lamp focused on the sample. The maximum intensity and the width at half maximum intensity were determined for all temperatures over a range of ±5% the full scale strip chart recorder "Y" axis.

The lifetimes of the complexes were determined at two emission wavelengths. The two wavelengths chosen were those corresponding to maximum emission intensities of the complex in PMM and methylcyclohexane. The emission decay was recorded by photographing the oscilloscope display or with the recorder output of the boxcar averager.

Results

Absorption and Emission Spectra. The low-temperature absorption and corrected emission spectra of the four S chelates are shown in Figures 2–5. For spectra at energies less than 28 000 cm^{-1} the solvent used was ETA and at energies greater than 28 000 cm^{-1} the solvent used was methylcyclohexane (MCH). Table I lists the energies of peak and shoulder maxima of the absorption spectra. The labels in column 2 of Table I are for reference and do not imply assignment of the transitions.

Several interesting features are apparent in these spectra. The maximum of band 2 of the absorption spectrum of

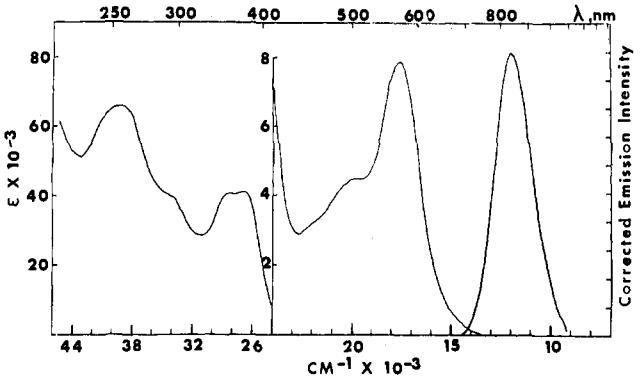

Figure 4. Low-temperature absorption and emission of $Rh(SSBB)_3$.

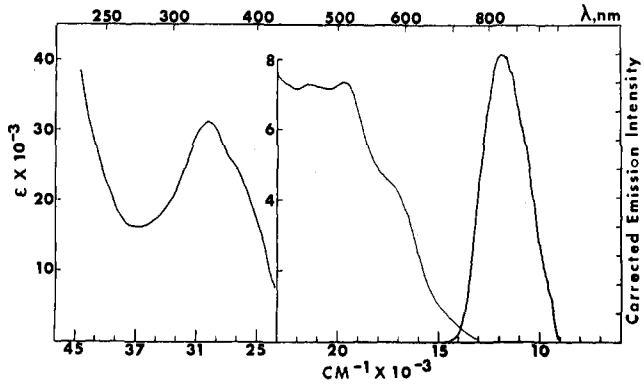

Figure 5. Low-temperature absorption and emission of $Ir(SSBB)_3$.

Table I. Absorption Data for the Sulfur Chelates in ETA or MCH

complex	band label	$\bar{\nu}$, cm^{-1} (83 K)	ϵ_{max} (296 K)
$Rh(SacSac)_3$	1	(14 000)[a,b]	3[c]
	2	19 600	7750
	3	(22 300)	3010
	4	(26 500)	3070
	5	(29 400)	5530
	6	(31 600)	11 200
	7	(36 100)	23 400
	8	(40 800)	60 200
	9	44 800	82 000
$Ir(SacSac)_3$	1	(16 100)	76[c]
	2a	19 500	5950
	2b	20 100	6380
	2c	21 400	7000
	3	(24 700)	1800
	4	(28 200)	4580
	5	(28 900)	5680
	6	(32 600)	12 200
	7	(33 800)	14 100
$Rh(SSBB)_3$	2	17 600	8220
	3	(20 200)	4400
	4a	26 500	40 700
	4b	28 300	40 600
	5	(34 200)	40 300
	6	39 000	66 000
$Ir(SSBB)_3$	1	(17 400)	4815
	2a	19 700	7850
	2b	21 600	7780
	3	(27 000)	26 200
	4	29 900	33 300

[a] Parentheses indicate shoulders. [b] This was a slight deflection of an optically dense solution. [c] Estimated molar extinction coefficients from 83 K absorption spectrum; corrected for overlapping higher energy absorption.

$Rh(SSBB)_3$ is red shifted 2000 cm^{-1} from the maximum of band 2 of the absorption spectrum of $Rh(SacSac)_3$ while the emission maximum of $Rh(SSBB)_3$ is only red shifted 600 cm^{-1} from that of $Rh(SacSac)_3$. Band 2 of $Ir(SacSac)_3$ is broadened and structured with respect to band 2 of $Rh(SacSac)_3$. The two SSBB complexes emission spectra overlap substantially with their respective absorption spectra. At the energy corresponding to 10% of the maximum emission intensity, the estimated molar extinction coefficients are 70 for $Rh(SSBB)_3$ and 330 for $Ir(SSBB)_3$.

Close examination of the corrected emission spectra shows an asymmetry about the maxima. In the case of the $Rh(SacSac)_3$ complex the absolute differences between the energy of the emission maximum and the energies of the intensities at one-half of the emission maximum are 960 and 1250 cm^{-1} for the blue side and red side, respectively. Therefore, it was assumed that the emission spectra of these complexes could be represented by the sum of two Gaussian functions. Approximately 150 data points from each emission curve were fit by a nonlinear least-squares iterative computer program, developed by Statistical Analysis Systems, Inc.[38]

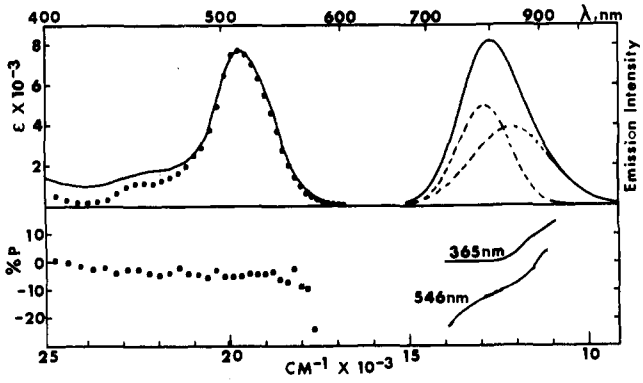

Figure 6. $Rh(SacSac)_3$. Upper half: • • •, corrected excitation spectrum; ---, components of the two-Gaussian fit; —, absorption and emission spectra. Lower half: excitation and emission polarization spectra.

Figures 6–9 show the best fit Gaussian functions for the emission spectrum of each of the compounds. Table II lists experimental and two Gaussian fit parameters for the compounds studied in solvents of ETA. The maxima from the two Gaussian fit data for the three solvents MCH, ETA, and PMM are shown in Figure 10. The symmetry of the $Ir(SSBB)_3$ emission spectrum in PMM suggests two Gaussians of similar width and height, a situation not amenable to the mathematical procedure used. The maximum of the $Ir(SSBB)_3$ emission spectrum in PMM is broadened with intensity only decreasing 5% over a 580-cm^{-1} (50 nm) interval.

Some general observations may be inferred from these data: (1) $Rh(SacSac)_3$, $Rh(SSBB)_3$, and $Ir(SSBB)_3$ behave similarly. (a) The narrower band is at higher energy than the broader band. (b) More polar solvents red shift both bands. (c) In MCH the narrower band is relatively the same energy for all three complexes. (2) $Ir(SacSac)_3$ is unique among the four complexes. (a) The narrower band is red shifted by a more polar solvent. (b) The broader band is blue shifted by a more polar solvent. (3) In PMM the energy of the broader band is approximately the same for all four complexes.

Polarization Spectra. The emission polarization spectra are shown on the bottom half of Figures 6–9. In the upper half of these figures the emission spectra and the components of the sum of two Gaussians are also depicted. In all four cases the presence of oppositely polarized components in emission polarization spectra verifies the two Gaussian fit model, therefore two overlapped spectra from two emitting states.

The excitation polarization spectra are also depicted in Figures 6–9. The emission wavelength monitored corresponded

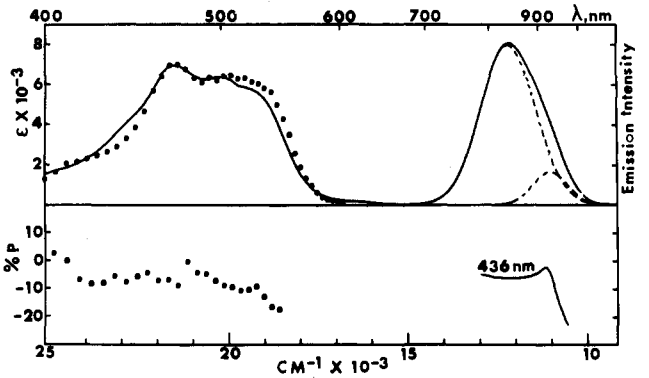

Figure 7. Ir(SacSac)$_3$. Upper half: • • •, corrected excitation spectrum; ---, components of the two-Gaussian fit; —, absorption and emission spectra. Lower half: excitation and emission polarization spectra.

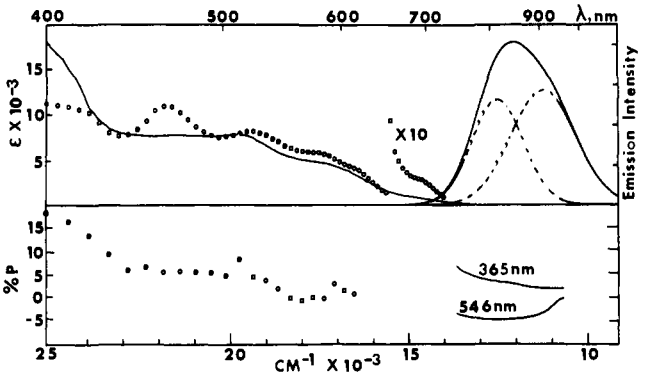

Figure 9. Ir(SSBB)$_3$. Upper half: • • •, corrected excitation spectrum; ---, components of the two-Gaussian fit; —, absorption and emission spectra. Lower half: excitation and emission polarization spectra.

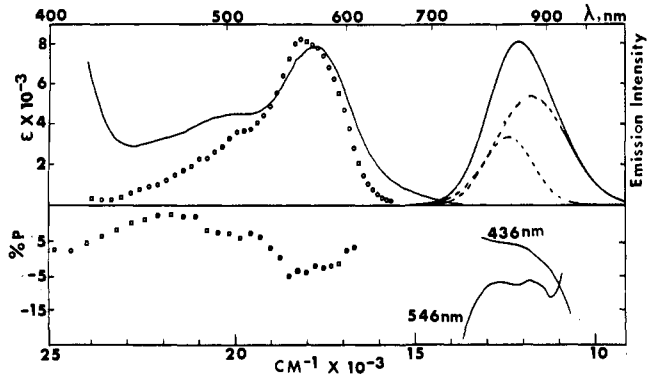

Figure 8. Rh(SSBB)$_3$. Upper half: • • •, corrected excitation spectrum; ---, components of the two-Gaussian fit; —, absorption and emission spectra. Lower half: excitation and emission polarization spectra.

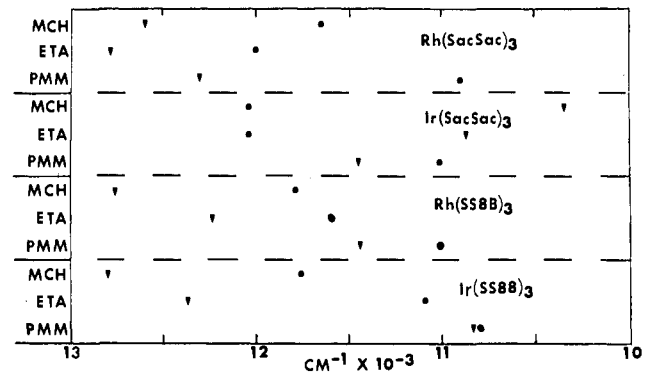

Figure 10. Positions of intensity maxima derived from the two-Gaussian fit model: ▼, narrower band; ●, broader band.

Table II. Emission Data for the Sulfur Chelates in ETA

compd	expt 1		two-Gaussian fit					
	$\bar{\nu}_{max}$, cm^{-1}	$\bar{\nu}_{1/2}$, cm^{-1}	I_1	$\bar{\nu}_{max(1)}$, cm^{-1}	$\bar{\nu}_{1/2(1)}$, cm^{-1}	I_2	$\bar{\nu}_{max(2)}$, cm^{-1}	$\bar{\nu}_{1/2(2)}$, cm^{-1}
Rh(SacSac)$_3$	12 600	2210	6.07	12 750	1710	4.77	12 000	2570
Ir(SacSac)$_3$	12 000	2080	9.77	12 040	1800	2.05	10 880	1130
Rh(SSBB)$_3$	12 000	2150	4.14	12 230	1580	6.59	11 590	2300
Ir(SSBB)$_3$	11 900	2800	6.45	12 370	1760	7.03	11 100	2130

to the experimental maximum. The band-pass was approximately 30 nm.

The excitation polarization spectra of all four complexes are complicated by the low values of P throughout the absorption region likely resulting from overlapping of bands and the polarization limits permitted for D_3 systems having planar oscillator emitter and absorbers.

Excitation Spectra. The low-temperature corrected excitation spectra are displayed in the upper half of Figures 6–9.[61] Corrected excitation intensities are shown at 5-nm intervals and are normalized with respect to the maximum molar extinction coefficient of band 2 of the absorption spectra. The low-temperature absorption spectra are included for reference.

For broad-band detection of emitted light the observed intensity of emitted light is given by the equation

$$I = I_{ex} g \Phi_p (1 - 10^{-\epsilon bc}) \qquad (5)$$

where I = intensity of emitted light, I_{ex} = intensity of exciting light, Φ_p = quantum yield, g = correction factor encompassing the fraction of light collected, transmission of filters, and the spectral response of the photomultiplier tube, ϵ = molar extinction coefficient, c = sample concentration, and b = path length of the sample. If $10^{-\epsilon bc} \geq 0.95$, then eq 5 may be approximated by the equation

$$I = 2.3 I_{ex} g \Phi_p (\epsilon bc) \qquad (6)$$

and the corrected excitation intensity is proportional to I/I_{ex}. When the quantum yield is invariant with the excitation wavelength,[39] the corrected excitation spectrum should be a replica of the absorption spectrum. Inspection of Figures 6–9 shows that the corrected excitation spectra do not duplicate the absorption spectra.

To permit greater sensitivity the spectrophotometer was used with a 450-W Xe lamp, and the uncorrected excitation spectra of Rh(SacSac)$_3$ and Rh(SSBB)$_3$ were recorded at two different emission wavelengths: 768 and 864 nm for Rh(SacSac)$_3$ and 784 and 844 nm for Rh(SSBB)$_3$. The excitation spectra at the shorter emission wavelength resembled those in Figures 6 and 8. The excitation spectra at the longer emission wavelength exhibit a better correlation with the absorption spectra. The intensity maxima corresponding to band 2 of the absorption spectra were not shifted for the longer emission wavelength. Also the ratio of maximum intensity to the minimum intensity, on the blue side of band 2, was smaller for the longer monitor wavelength than the shorter monitor wavelength.

Table III. Lifetimes of the S Chelates

compd	linear fit parameters	nonlinear fit parameters	linear fit parameters	nonlinear fit parameters
		A. In MCH		
$Rh(SacSac)_3$	λ 764 nm		λ 842 nm	
	$\tau = 24.3 \pm 1.1$ [a]	$I_1 = 4.8 \pm 2.1$	$\tau = 18.0 \pm 0.5$	$I_1 = 3.9 \pm 0.8$
	$I_0 = 6.8 \pm 0.5$	$\tau_1 = 10.9 \pm 4.1$	$I_0 = 6.5 \pm 0.3$	$\tau_1 = 6.7 \pm 1.6$
	$R = 0.993\ 81$	$I_2 = 4.1 \pm 2.3$	$R = 0.996\ 61$	$I_2 = 4.5 \pm 1.0$
		$\tau_2 = 30.8 \pm 9.0$		$\tau_2 = 22.4 \pm 3.0$
$Ir(SacSac)_3$	λ 764 nm		λ 842 nm	
	$\tau = 1.57 \pm 0.06$	$I_1 = 7.94 \pm 2.2$	$\tau = 1.02 \pm 0.04$	$I_1 = 2.64 \pm 0.1$
	$I_0 = 7.39 \pm 0.4$	$\tau_1 = 0.37 \pm 0.1$	$I_0 = 5.5 \pm 0.3$	$\tau_1 = 1.07 \pm 10^{17}$
	$R = 0.995\ 72$	$I_2 = 6.1 \pm 0.6$	$R = 0.996\ 13$	$I_2 = 2.6 \pm 0.0$
		$\tau_2 = 1.75 \pm 0.1$		$\tau_2 = 1.07 \pm 10^{17}$
$Rh(SSBB)_3$	λ 801 nm		λ 854 nm	
	$\tau = 63.3 \pm 0.6$	$I_1 = 16 \pm 125$	$\tau = 49.2 \pm 1.4$	$I_1 = 4.4 \pm 1.2$
	$I_0 = 9.82 \pm 0.08$	$\tau_1 = 3.8 \pm 6.4$	$I_0 = 7.7 \pm 0.1$	$\tau_1 = 13.0 \pm 6.5$
	$R = 0.999\ 74$	$I_2 = 9.76 \pm 0.1$	$R = 0.997\ 82$	$I_2 = 6.4 \pm 1.1$
		$\tau_2 = 63.6 \pm 0.9$		$\tau_2 = 55.8 \pm 3.1$
$Ir(SSBB)_3$	λ 754 nm		λ 844 nm	
	$\tau = 4.61 \pm 0.06$	$I_1 = 3.2 \pm 0.2$	$\tau = 2.71 \pm 0.05$	$I_1 = 3.7 \pm 2.7$
	$I_0 = 6.7 \pm 0.2$	$\tau_1 = 4.8 \pm 260$	$I_0 = 5.8 \pm 0.3$	$\tau_1 = 3.4 \pm 0.2$
	$R = 0.999\ 35$	$I_2 = 3.2 \pm 0$	$R = 0.998\ 62$	$I_2 = 2.7 \pm 3.6$
		$\tau_2 = 4.85 \pm 260$		$\tau_2 = 1.5 \pm 1.0$
		B. In PMM		
$Rh(SacSac)_3$	λ 773 nm		λ 819 nm	
	$\tau = 12.2 \pm 0.3$	$I_1 = 1.5 \pm 0.7$	$\tau = 10.6 \pm 0.2$	$I_1 = 2.0 \pm 0.6$
	$I_0 = 4.97 \pm 0.09$	$\tau_1 = 4.2 \pm 1.3$	$I_0 = 5.6 \pm 0.1$	$\tau_1 = 4.3 \pm 0.8$
	$R = 0.997\ 50$	$I_2 = 3.8 \pm 0.7$	$R = 0.997\ 93$	$I_2 = 4.05 \pm 0.6$
		$\tau_2 = 15.3 \pm 2.2$		$\tau_2 = 13.2 \pm 1.2$
$Ir(SacSac)_3$	λ 754 nm		λ 844 nm	
	$\tau = 1.88 \pm 0.08$	$I_1 = 1.7 \pm 0.4$	$\tau = 0.86 \pm 0.04$	$I_1 = 3.8 \pm 10^{-4}$ [b]
	$I_0 = 4.8 \pm 0.3$	$\tau_1 = 0.4 \pm 0.1$	$I_0 = 8.2 \pm 0.6$	$\tau_1 = 0.34$
	$R = 0.993\ 10$	$I_2 = 4.1 \pm 0.4$	$R = 0.995\ 11$	$I_2 = 8.6$
		$\tau_2 = 2.1 \pm 0.2$		$\tau_2 = 0.81$
$Rh(SSBB)_3$	λ 814 nm		λ 857 nm	
	$\tau = 20.1 \pm 0.5$	$I_1 = 3.5 \pm 0.1$	$\tau = 18.2 \pm 0.6$	$I_1 = 6.84$ [b]
	$I_0 = 7.0 \pm 0.2$	$\tau_1 = 20.2 \pm 1.1$	$I_0 = 6.6 \pm 0.3$	$\tau_1 = 13.2$
	$R = 0.997\ 56$	$I_2 = 3.5 \pm 0$	$R = 0.996\ 05$	$I_2 = 0.67$
		$\tau_2 = 20.2 \pm 0$		$\tau_2 = 257$
$Ir(SSBB)_3$	λ 773 nm		λ 854 nm	
	$\tau = 3.42 \pm 0.03$	$I_1 = 5.31 \pm 0.8$	$\tau = 1.89 \pm 0.09$	$I_1 = 7.7 \pm 1.2$
	$I_0 = 8.88 \pm 0.04$	$\tau_1 = 0.9 \pm 0.4$	$I_0 = 8.28 \pm 0.1$	$\tau_1 = 0.6 \pm 0.2$
	$R = 0.999\ 49$	$I_2 = 8.9 \pm 1.9$	$R = 0.999\ 68$	$I_2 = 8.2 \pm 2.4$
		$\tau_2 = 3.4 \pm 0.4$		$\tau_2 = 1.9 \pm 0.3$

[a] Lifetimes are in units of μs and error limits are the 95% confidence level. [b] The procedure failed to converge; therefore no error can be assigned.

The corrected excitation spectra of the iridium(III) S chelates increased the resolution of three absorption bands: band 3, a weak shoulder, of $Ir(SacSac)_3$ is more pronounced, band 2c of $Ir(SSBB)_3$ is much more pronounced, and, for $Ir(SSBB)_3$, a shoulder not observed in the absorption spectrum appears at 14 500 cm^{-1}.

Decay Measurements. The decay of an emitting excited state following pulsed excitation is a first-order process giving a single decay constant, τ, normally independent of the emission wavelength monitored.

Although the decay curves for all materials appear exponential, the lifetimes are dependent upon the emission wavelength monitored. Since different "lifetimes" at two wavelengths were observed, the assumption that the observed decrease of intensity with time could be rationalized by a sum of two exponents was tested. The nonlinear procedure used to resolve the emission band into two Gaussians was used to evaluate the parameters of the equation

$$I = I_1 \exp(-t/\tau_1) + I_2 \exp(-t/\tau_2) \quad (7)$$

Table III lists the lifetimes calculated at two different wavelengths for the complexes in solvents of MCH and PMM, respectively. Linear and nonlinear fit parameters are both given. Table IV lists the linear fit parameters of the complexes at the emission intensity maxima of the complexes in ETA.

Some anomalies are apparent in the data of the nonlinear fit of Table III. A long-lifetime (τ_2) component is present at the two different wavelengths but agreement between these τ_2's is poor. A statistical "t" [40] test indicates that the difference between the two long-lifetime components cannot be accounted for by random error. Calculation of the ratio of the intensities from the two Gaussian fit parameters at the given wavelengths is not consistent with the ratio of intensities at time = 0 for the decay data. The error limits on the short-lifetime (τ_1) components are large.

One possible cause of these anomalies is the inability of this nonlinear method to adequately resolve components whose lifetimes are separated by a factor of less than 3 within the uncertainty of the experimental data.[41,42] For example, intensity-time data were calculated for the parameters $I_1 = 5.0$, $\tau_1 = 20.0$, $I_2 = 5.0$, and $\tau_2 = 30.0$ with the calculated values of I rounded to the nearest hundredth. The nonlinear procedure calculated values of $I_1 = 3.2 \pm 6.6$, $\tau_1 = 32.7 \pm 15$, $I_2 = 6.8 \pm 6.6$, and $\tau_2 = 21.5 \pm 4.3$ while a linear fit, log (I) vs. t, gave

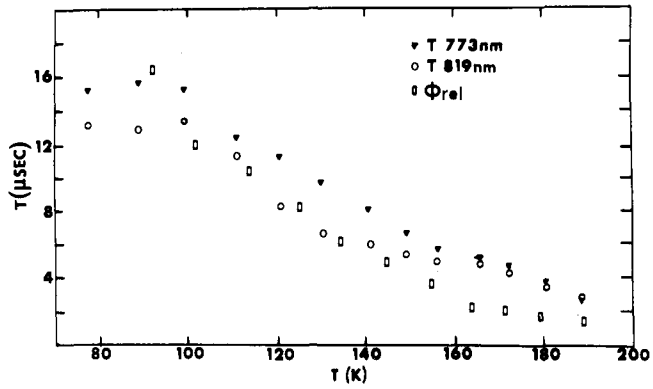

Figure 11. Plot of lifetimes and relative quantum yield of $Rh(SacSac)_3$ in PMM vs. temperature.

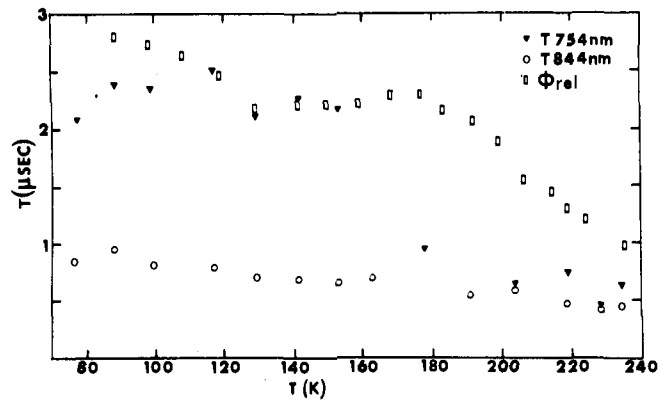

Figure 12. Plot of lifetimes and relative quantum yield of $Ir(SacSac)_3$ in PMM vs. temperature.

Table IV. Low-Temperature Lifetimes of the S Chelates in ETA

compd	lifetime, μs	compd	lifetime, μs
$Rh(SacSac)_3$	23.8	$Rh(SSBB)_3$	30.3
$Ir(SacSac)_3$	1.1	$Ir(SSBB)_3$	2.5

calculated parameter values of $I_0 = 9.85 \pm 0.04$, $\tau = 25.1 \pm 0.1$, and $R = 0.999\,95$.

The short-lifetime component could also be distorted by the rise time of the measuring system. Although this effect can be minimized for the monoexponential system through deconvolution[43] using the equation

$$I = \frac{I_0[\exp(-t/\tau) - \exp(-t/\mathrm{RC})]}{(1 - \mathrm{RC}/\tau)} \qquad (8)$$

RC = RC time constant of the circuit

the number and precision of the input data points preclude such a procedure here. To diminish this RC time constant effect on the decay data, the fit intensity point was measured at a time that was greater than the maximum of the decay curve's "rise time". In most cases this first point corresponded to a time that was approximately one-half of the short-lifetime component. Therefore the contribution to the total intensity by this short component was reduced leading to greater error in estimates of the parameters of this component.

A third possibility that the true rate expression is the sum of three or more exponentials can be discounted since attempts to fit data to a three-exponential sum gave the same parameters as the two-exponential fit.

Variable Temperature Results. The emission spectrum of $Rh(SSBB)_3$ in decalin was recorded at five different temperatures between 77 and 120 K. The intensity decreased rapidly over this range with large broadening of the emission band and, at 120 K, was too weak to measure; consequently other solvents must be used. Although decalin has a glass transition point of approximately 200 K, its macroscopic viscosity at 120 K is greater than or equal to the macroscopic viscosity of MCH at 77 K.[44] Therefore intermolecular relaxation processes may result from microscopic viscosity effects.

Polymeric hosts provide a superior media for variable temperature measurements since the microscopic viscosity is relatively constant over a large temperature range. Figures 11 and 12 illustrate the temperature-dependent results of the long-lifetime components and relative quantum yields of the SacSac chelates. Short-lifetime components were too scattered to provide meaningful results.

The temperature dependence of τ is given by the equation

$$1/\tau = k_r + A \exp(-E_a/kT) \qquad (9)$$

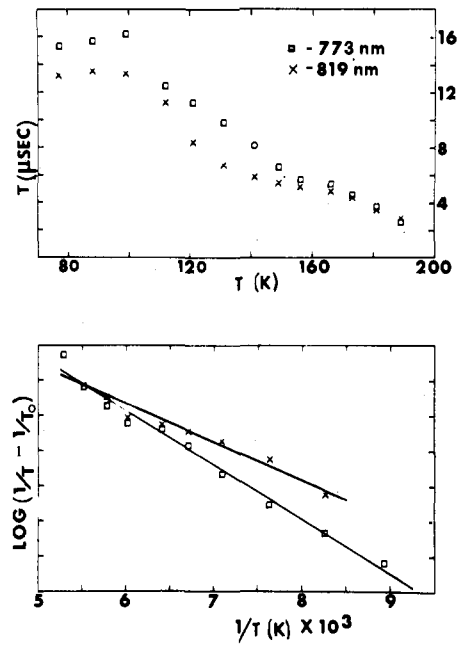

Figure 13. Arrhenius plot of lifetime vs. temperature of $Rh(SacSac)_3$ in PMM.

where E_a = the activation energy, k = Boltzmann constant, A = preexponential term, and T = the temperature in K. Therefore a plot of ln $(1/\tau - 1/\tau_0)$ vs. $1/T$, where τ_0 is the temperature-independent lifetime, should have a slope equal to $-E_a/k$. Figure 13 shows such an Arrhenius plot for $Rh(SacSac)_3$. Calculated values of E_a are given in Table V for the two long-lifetime components of the S chelates. By analogy the temperature dependence of the quantum yield, Φ, is given by the equation

$$1/\Phi = 1 + A' \exp(-E_a/kT) \qquad (10)$$

After the low-temperature relative quantum yield was normalized to unity, the activation energies calculated from the relative quantum yields are also included in Table V. The rate constant, $k_r = \Phi/\tau\Phi_{isc}$, where Φ_{isc} is the yield for intersystem crossing, is independent of temperature in most systems.[45] Any variation with temperature reflects a temperature dependence of Φ_{isc}. The ratio of $\Delta\Phi/\Delta\tau$ is given in Table V as increases, decreases, or constant.

Discussion

The experimental results indicate that the luminescence of the trisdithio β-diketonate complexes of Rh(III) and Ir(III) is unique, i.e., asymmetry of the emission spectra and emission

Table V. Activation Energies for the S Chelates in PMM

compd	E_a (from τ_2 shorter λ)	E_a (from τ longer λ)	E_a (from Φ_{rel})	$\Delta\Phi/\Delta\tau_2$ short λ	$\Delta\Phi/\Delta\tau_2$ long λ
$Rh(SacSac)_3$	6.4×10^3 J/mol ($540\ cm^{-1}$)	4.6×10^3 J/mol ($380\ cm^{-1}$)	6.6×10^3 J/mol ($550\ cm^{-1}$)	decreases	decreases
$Ir(SacSac)_3$	*a*	3.7×10^3 J/mol ($310\ cm^{-1}$)	1.2×10^4 J/mol ($1030\ cm^{-1}$)	increases	decreases
$Rh(SSBB)_3$	9.9×10^3 J/mol ($840\ cm^{-1}$)	8.5×10^3 J/mol ($710\ cm^{-1}$)	8.6×10^3 J/mol ($720\ cm^{-1}$)	decreases	decreases
$Ir(SSBB)_3$	4.1×10^3 J/mol ($340\ cm^{-1}$)	4.4×10^3 J/mol ($370\ cm^{-1}$)	5.4×10^3 J/mol ($450\ cm^{-1}$)	increases	increases

[a] The lifetime is nearly at one constant level at lower temperatures and at another constant level at higher temperatures.

Table VI. Assignments of the Absorption Transitions

compd	band	assignment
$Rh(SacSac)_3$	2	$\Pi e \leftarrow \Pi\Pi$
	3	$\Pi\Pi^* \leftarrow \Pi\Pi$
	9	$\Pi\Pi^* \leftarrow \Pi\Pi$
$Ir(SacSac)_3$	2c	$\Pi e \leftarrow \Pi\Pi$
	3	$\Pi\Pi^* \leftarrow \Pi\Pi$
	7	$\Pi\Pi^* \leftarrow \Pi\Pi$
$Rh(SSBB)_3$	2	$\Pi e \leftarrow \Pi\Pi$
	3	$\Pi\Pi^* \leftarrow \Pi\Pi$
	6	$\Pi\Pi^* \leftarrow \Pi\Pi$
$Ir(SSBB)_3$	2a	$\Pi e \leftarrow \Pi\Pi$
	2b	$\Pi\Pi^* \leftarrow \Pi$
	4	$\Pi\Pi^* \leftarrow \Pi\Pi$

wavelength dependent lifetimes. This anomalous behavior could be the result of intrinsic intramolecular (multiple emission) or extrinsic environmental effects (including "impurities"). The results will be discussed in terms of these two hypotheses.

Environmental Effects. An Impurity. Assuming that the anomalies arise from an impurity, that impurity likely must be unique for each complex since a common lifetime component could not be extracted for the materials. The most probable impurity would be some combination of monothio β-diketonate and dithio β-diketonate ligands coordinated to the metal ion. Since the SacSac complexes were prepared by bubbling H_2S into a solution of the metal ion and acetylacetone, such an impurity is possible. However, separation of $Rh(SacSac)_3$ and tris(monothioacetylacetone)rhodium(III) has been accomplished by ligand-phase chromatography[46] and here all complexes were purified by liquid-phase chromatography. Moreover, IR spectra revealed no frequencies characteristic of the carbonyl stretch. Such an impurity in the SSBB complexes is even less probable since the SSBB complexes were prepared from the oxidized form of dithiodibenzoylmethane and the metal ion. The exhaustive chromatographic examination of the SSBB materials (Experimental Section) should preclude any other impurity here. Finally, if the two-Gaussian fit of the emission band does resolve two impurity component emissions, then the comparable intensity of the two components would necessitate that the emission quantum yield of the impurity be an order of magnitude larger than that of the pure component. Such behavior would be unique, in particular when repeated for all four compounds.

Attempts to photolyze the materials at low temperature resulted in no discernible changes in absorption or emission properties. Although the presence of an impurity can never be entirely discounted, the presence of one here appears inconsistent with the data.

Instrumental Artifacts. Multiexponential decay can result from photophysical processes[47] resulting from rotational relaxation times. Since experimental determination of rotational diffusion constants necessary for assessment of this mechanism is difficult, a calculation of τ_{rot} was done from the Stokes relationship and single crystal data[48] for $Rh(SacSac)_3$. This result verified that such a mechanism was not the cause of the multiexponential decay. Finally, using the same experimental system, the decay curves of $Cr(acac)_3$ and $[Rh(phen)_2Cl_2]^+$ at 77 K were exponential over 2-3 lifetimes.

Solvent Cage Heterogeneity. As discussed above, the relaxation of excited molecules in rigid media is much faster than the rotational relaxation rate. Therefore the possibility arises that in rigid media the solute can exist in a variety of different solvent sites. Polar aromatic hydrocarbons such as indole[49] in polar solvents show a dependence of the emission maximum upon excitation wavelength. Excitation into the red side of indole's lowest absorption band red shifts the emission maximum from that excited with shorter wavelengths. The solute molecules in selected sites, where the 0-0′ transition is lower in energy than the average of all the solutes' 0-0′ energy, is selectively excited with lower wavelengths. Upon warming the solution to fluidity this "red edge" effect disappears. Nonpolar aromatic hydrocarbons do not exhibit this effect.

This effect has been used to rationalize the fast decay component observed in $[Cr(CN)_6]^{3-}$ [50] at low temperatures. This compound has been reported to fluoresce but further investigation revealed that the short-lifetime component was only present for excitation into the red side of the lowest absorption band. Also this fast component disappeared upon warming the solution to fluidity. Similarly, for $[Cr(urea)_6]^{3+}$, the prompt fluorescence that had been reported is also ascribed to this solvent cage effect.[51] This compound exhibits the multiexponential at most excitation wavelengths and not just the red side of the lowest absorption peak.

The emission maximum of $Rh(SSBB)_3$ in PMM was monitored as a function of excitation wavelength. The emission maximum was at 855 nm for the 365-, 436- (blue side of band 2), and 579-nm (red side of band 2) excitations but for 546-nm excitation just to the blue side of band 2, the emission maximum was at 840 nm. Thus a "red edge" effect is not observable for this case.

For the indole and Cr^{3+} cases the solvent used was a water-ethylene glycol mixture. In such a solvent strong dipole-dipole or dipole-charge interactions are present. However for our S chelates with no net dipole or charge, dissolved in less polar solvents, solvent-solute interactions presumably would be less significant than for indole or Cr^{3+} cases.

Intramolecular Processes. Assignment of the Transitions. Although the S chelates have D_3 symmetry, all notation is given in O_h microsymmetry. Within the ligand field approximation four distinct orbital descriptions of the absorption transitions are possible: (1) $t_2^5e \leftarrow t_2^6$, (2) $t_2^5\Pi^* \leftarrow t_2^6$, (3) $\Pi e \leftarrow \Pi\Pi$, (4) $\Pi\Pi^* \leftarrow \Pi\Pi$. Table VI lists orbital assignments proposed on the basis of intensity, shape, and substituent shifts.

The magnitude of the molar extinction coefficient for bands assigned as CTTM, charge transfer to metal, eliminates a d-d* type absorption. Although the free ligand or a filled shell metal complex of SacSac have not been isolated, the Zn^{2+}, Cd^{2+}, and

Hg^{2+} complexes of i have been synthesized.[52] The lowest energy absorption band of these complexes is between 24 500 and

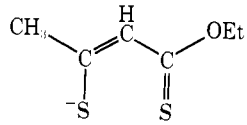

i

24 000 cm^{-1} with ϵ ranging between 11 500 and 16 200. The absorption spectrum of the two-electron reduction product of ($SSBB^+$) has also been recorded and this anion has a maximum at 20 800 cm^{-1} with ϵ = 25 000. Thus the bands assigned as CTTM are not Π-Π^* since the known Π-Π^* transition is at higher energy. Charge transfer absorption bands can be correlated with the ease of oxidation and reduction of the metal and ligands.[53,54] Since the oxidation potential of Ir^{3+} is less than that of Rh^{3+}, then the CTTL band for iridium(III) complexes should be at lower energy than that of the rhodium(III) complexes. Since the ligands are easily oxidized and the e orbital of rhodium is lower in energy than the e orbital of iridium, therefore the CTTM assignment is consistent with the spectra.

The intensity of the absorption transition is also consistent with this assignment since CTTM transitions for the heavy metal hexahalo complexes[54] have molar extinction coefficients in the range 2000-70 000.

The shoulder assigned as a Π-Π^* transition could be assigned as d-d* but the large red shift from $Rh(SacSac)_3$ to $Rh(SSBB)_3$ is inconsistent with the small difference expected in the crystal field strength of SacSac and SSBB. This band is nearly isoenergetic with the band in the SSBB anion assigned as Π-Π^* absorption. Although the apparent maximum of this band of $Ir(SacSac)_3$ is blue shifted from the others, the true maximum could be obscured by the CTTM absorption band.

Unassigned Transitions. From the spectra of $Rh(dtp)_3$, $Rh(dtc)_3$, etc., the d-d* transition for these materials would be predicted in the 19 000-23 000-cm^{-1} region. Assuming that the CTTM and Π-Π^* assignments are correct, then the d-d* transition must be obscured by these transitions. Bands 2a and 1 of $Ir(SacSac)_3$ and $Ir(SSBB)_3$, respectively, are not the d-d transitions because the corresponding transitions in the Rh^{3+} complexes would be discernible on the red side of the CTTM transition. These transitions in the Ir^{3+} complexes could result from one of two possibilities: (1) The degeneracy in the CTTM state is reduced by geometrical perturbations. (2) The transition arises from a d-Π^* configuration. The corresponding transition in the Rh^{3+} complexes would occur at higher energies.

Bands 1 of $Ir(SacSac)_3$ and $Rh(SacSac)_3$ are most likely spin-forbidden transitions but their orbital origin is not apparent.

Emission Transitions. The two-Gaussian fit, multiple lifetimes, and polarization spectra indicate that the emission occurs from two different states. The half-width of the broader of the bands from the two-Gaussian fit suggests assignment of this band as ^{3}(d-d) $\rightarrow$ $^1A_1$, while from the CTTM visible absorption band position and the solvent dependence of the emission the other band is assigned as $^3(\Pi\text{-}d^*) \rightarrow {}^1A_1$.

Emission from a $^3(\Pi\text{-}d^*)$ state has never been reported for a d^6 complex; consequently characterization of the luminescence based on prior observation is not possible. However, a large Stokes' shift is expected since an electron is promoted to an antibonding σ orbital. Since the emission of all other d^6 complexes is a spin-forbidden process, the emitting (Π-d*) state is also assumed to be a triplet consistent with the magnitude of the experimental lifetime. Although the spin may not be a valid quantum number, the present data precludes evaluating spin-orbit coupling effects to quantitatively evaluate this factor.

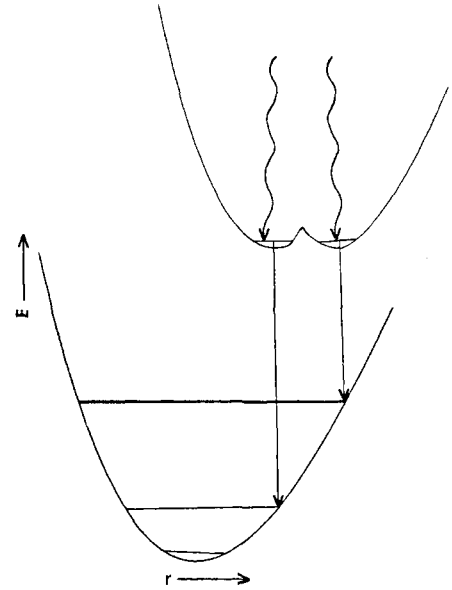

Figure 14. Proposed pathways of deactivation of the excited states of the S chelates.

Assignment of the emission and absorption transitions as transitions between states deriving from extensively mixed orbitals was suggested (Introduction) as a possibility for these molecules. However, two types of evidence argue against such an assignment: (1) Band positions can be satisfactorily rationalized within the limits of a ligand field model (Π-Π^* and charge transfer absorption bands and the d-d emission are consistent with a d-d model). (2) The existence of a multiple emission, implying lack of communication between emitting channels and states, would appear to be less likely for two states deriving from molecular orbitals having comparable metal d and ligand Π character.

The electrochemistry reported for the $Rh(SacSac)_3$ complex[55] indicates a structural instability associated with reduction of this species, consistent with expectation for addition of the electrons into a d_σ-type orbital (therefore a ligand field type model). Similar data[56] indicate that on the polarographic time scale the $Ir(SacSac)_3$ complex, in contrast to the $Rh(SacSac)_3$ case, undergoes two reversible one-electron reductions implying some greater stability of this reduced species.

Deactivation of Excited States. Figure 14 shows a schematic representation of the proposed pathways of deactivation from the lowest excited states in the S chelates. Based on Figure 15 the ligand substituent might be expected to significantly alter the emission. That is, the ^{3}(d-d) should be lowered in energy only slightly with phenyl substitution of methyl while the $^3(\Pi\text{-}d^*)$ should be lowered relatively more. However, inspection of the maxima of the two-Gaussian fit data reveals that corresponding bands for the same metal center with different ligands are displaced about equally. This paradox can be explained in two ways.

(1) The accuracy of the maxima may be limited. The standard deviation from the mathematical fit was on the order of 50-150 cm^{-1}. As evidenced by the polarization data, the general spectral range of each Gaussian is correct but extension to precise prediction of peak maxima and band widths may be limited.

(2) The special shifts expected presume that the displacement with respect to the reaction coordinate of the potential energy surfaces is unaffected by substituents. This assumption may not be valid as evidenced in spectral data of the acac and

dbm complexes of Be^{2+}, Al^{3+}, and Zn^{2+}.[59] The lowest energy absorption band of these complexes is red shifted 6500 cm^{-1} by substitution of dbm for acac while the 0-0′ phosphorescence band is only red shifted 4600 cm^{-1}.

The excitation spectra indicate that the two emitting states are populated by different pathways.

The excitation spectra data imply that (1) Φ_p (broader band) is nearly independent of the exciting wavelength; (2) Φ_p (narrower band) is dependent upon the exciting wavelength.

Rate Expressions. Figure 15 indicates the kinetic model for the deactivation of the two lowest excited states. Since k_r and k_{nr} cannot be uncoupled from one another without absolute quantum yields, let $(k_{r1} + k_{nr1})$ and $k_{r2} + k_{nr2})$ equal k_1 and k_2, respectively. Also n_i is the number of molecules with excited state i, and n_i^0 is the number at time $t = 0$ after flash excitation. Although rate expressions would simplify if some $n_i^0 = 0$, there is no basis to assume this with the present data.

Case 1:

$$k_3 = k_{-3} = 0$$

$$n_1 = n_1^0 \exp(-k_1 t) \text{ and } n_2 = n_2^0 \exp(-k_2 t)$$

$$I(t) = I_1 \exp(-k_1 t) + I_2 \exp(-k_2 t)$$

Case 2:

$$k_3 > 0, k_{-3} = 0$$

$$\frac{dn_1}{dt} = -(k_1 + k_3)n_1, \frac{dn_2}{dt} = -k_2 n_2 + k_3 n_1$$

$$n_1 = n_1^0 \exp[-(k_1 + k_3)t]$$

$$n_2 = \frac{k_3 n_1^0 \exp[-(k_1 + k_3)t]}{-(k_1 + k_3 - k_2)} + \frac{n_2^0 + n_1^0 k_3}{(k_1 + k_3 - k_2)} \exp(-k_2 t)$$

$$I(t) = I_1 \exp[-(k_1 + k_3)t] + I_2 \exp[-(k_2 t)]$$

Case 3:[58]

$$k_3 \text{ and } k_{-3} > 0$$

$$\frac{dn_1}{dt} = -(k_1 + k_3)n_1 + k_{-3} n_2$$

$$\frac{dn_2}{dt} = -(k_2 + k_{-3})n_2 + k_3 n_1$$

$$n_1 = a_{11} \exp(-\lambda_1 t) + a_{12} \exp(-\lambda_2 t)$$

$$n_2 = a_{21} \exp(-\lambda_1 t) + a_{22} \exp(-\lambda_2 t)$$

$$\lambda_{1,2} = \tfrac{1}{2}(k_1 + k_2 + k_3 + k_{-3}) \pm [(k_1 + k_2 + k_3 + k_{-3})^2 - 4(k_1 k_2 - k_3 k_{-3})]^{1/2}$$

and the a_{ij} are combinations of the k_i's and n_i^0's

$$I(t) = I_1 \exp(-\lambda_1 t) + I_2 \exp(-\lambda_2 t)$$

In all three cases the experimental intensity will be the sum of two exponents. The measured k_i's or τ_i's should be the same at different wavelengths while the ratio of I_1/I_2 should vary with wavelength. As indicated in the Results, long and short τ's are calculated at two different wavelengths but the two long τ's are different, inconsistent with the model.

Although the possibility that different site symmetries cause the wavelength-dependent τ cannot be totally discounted, another source of the discrepancy seems more probable. For both cases 2 and 3 above, the preexponential factors are complex combinations of rate constants such that a rise time can be associated with the population of one of the two emitting levels. Such a circumstance occurs at low temperature, for Cr^{3+} systems showing fluorescence and phosphorescence.[51,59] Sample calculations of the long lifetime using the nonlinear calculation method demonstrate that an incomplete data set (no rise portion) will generate different sets of rate constants

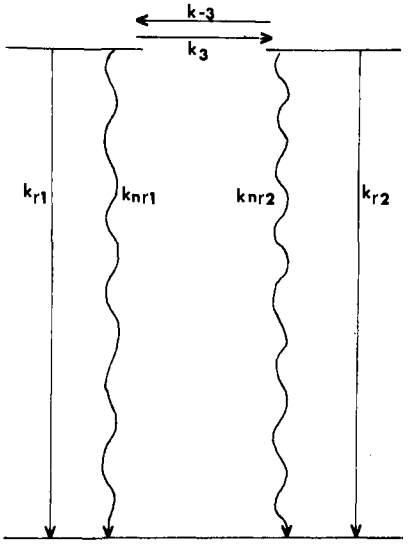

Figure 15. Kinetic model for the deactivation of the excited states of the S chelates.

for different wavelengths. Further, experimental rise times were measured for the $Ir(SSBB)_3$ (complex having the shortest τ) at 773 and 854 nm and gave values of 0.474 ± 0.006 and 0.419 ± 0.003 μs, respectively. The invariance of system RC constant with wavelength therefore does verify that the measured variation in τ with wavelength does result from the presence of a true rise time.

If case 2 or 3 is the correct mechanism and the temperature dependences of k_{nr1}, k_{nr2}, k_3, and k_{-3} are of comparable magnitude, then the measured activation energies cannot have any simple physical interpretation. If the lifetimes are determined by only one of the nonradiative rate constants, then the measured activation energies could be correlated with vibrational deactivation processes.

Summary

Luminescence spectra and lifetimes have been measured for four trisdithioketone complexes of Rh^{3+} and Ir^{3+}. The emission spectra are broad and asymmetric and overlap substantially with absorption spectra. The asymmetric emission bands can, for all compounds, be resolved into two Gaussian components, consistent with the two-exponential fit of the decay-curve data. Emission polarization spectra determined for the four sulfur chelate complexes of Rh(III) and Ir(III) verify the presence of two emitting states for each of these compounds. Excitation polarization spectra are generally depolarized for these D_3 systems suggesting the overlap of oppositely polarized emitting states.

Analysis of the origin of this unique behavior indicates that the luminescence is an intrinsic intramolecular phenomena, multiple emission. Band shapes and positions are used to assign the emission band as arising from noncommunicating quasi-degenerate d-d and charge transfer (Π-d*) states.

Excitation spectra verify the existence of independent pathways of population for the two emitting states. Moreover, emission from the "dd" (broader) band state appears nearly independent of excitation wavelength while the charge transfer emission is dependent upon excitation wavelength.

The decay data can be interpreted as indicating the presence of a finite rise time for the emission of one of the emitting states. The complex form of the kinetics scheme precludes interpretations of the measured activation energies.

Ultimately increased sensitivity of the detection system in the red region should enable shorter system response time. Consequently, decay times measured in the wings of the emission band may permit unraveling of the complex decay

schemes. Time-resolved emission and excitation spectra could permit additional elaboration of the relaxation pathway and verification of the assignment of the broad and narrow emission bands.

References and Notes

(1) L. S. Forster in "Transition Metal Chemistry", Vol. 5, R. L. Carlin, Ed., Marcel Dekker, New York, 1969.
(2) L. S. Forster in "Concepts in Inorganic Photochemistry", A. Adamson and P. Fleischauer, Eds., Wiley, New York, 1975.
(3) P. D. Fleischauer, A. W. Adamson, and G. Sartori, *Prog. Inorg. Chem.*, **17**, 1 (1972).
(4) D. J. Robbins and A. J. Thomson, *Mol. Phys.*, **25**, 1103 (1973).
(5) M. K. DeArmond, *Acc. Chem. Res.*, **7**, 309 (1974).
(6) G. A. Crosby, *Acc. Chem. Res.*, **8**, 231 (1975).
(7) J. E. Hillis and M. K. DeArmond, *J. Lumin.* **4**, 273 (1971).
(8) Y. Ohashi, K. Yoshihora, and S. Nogukura, *J. Mol. Spectrosc.*, **38**, 43 (1971).
(9) W. Halper and M. K. DeArmond, *J. Lumin.*, **5**, 225 (1972).
(10) R. J. Watts, M. J. Brown, B. G. Griffith, and J. S. Harrington, *J. Am. Chem. Soc.*, **97**, 6029 (1975).
(11) R. J. Watts, B. G. Griffith, and J. S. Harrington, *J. Am. Chem. Soc.*, **98**, 674 (1976).
(12) R. J. Watts and D. Missimer, *J. Am. Chem. Soc.*, in press.
(13) P. J. Giordano, S. M. Fredericks, M. S. Wrighton, and D. L. Morse, *J. Am. Chem. Soc.*, **100**, 2257 (1978).
(14) C. K. Jorgensen, *J. Inorg. Nucl. Chem.*, **24**, 1571 (1962).
(15) J. E. Hillis and M. K. DeArmond, *Chem. Phys. Lett.*, **10**, 325 (1971).
(16) F. Weigert, *Verh. Dtsch. Phys. Ges.*, 1, 100 (1920).
(17) S. I. Vavilov and V. L. Levshin, *Z. Phys.*, **16**, 136 (1923).
(18) F. Perrin, *J. Phys. Radium*, **7**, 390 (1926).
(19) A. Jablonski, *Z. Phys.*, **96**, 236 (1935).
(20) A. C. Albrecht and W. T. Simpson, *J. Am. Chem. Soc.*, **77**, 4454 (1955).
(21) A. C. Albrecht, *J. Mol. Spectrosc.*, **6**, 84 (1961).
(22) M. A. El-Sayed, *J. Chem. Phys.*, **38**, 2834 (1963).
(23) M. A. El-Sayed, *Acc. Chem. Res.*, 1, 8 (1968).
(24) T. Pavlopoulos and M. A. El-Sayed, *J. Chem. Phys.*, **41**, 1082 (1964).
(25) M. A. El-Sayed, *J. Chem. Phys.*, **43**, 2864 (1965).
(26) Y. Kanda, J. Stanislaus, and E. C. Lim, *J. Am. Chem. Soc.*, **91**, 5085 (1969).
(27) Y. H. Li and E. C. Lim, *Chem. Phys. Lett.*, **7**, 15 (1970).
(28) M. E. Long and E. C. Lim, *Chem. Phys. Lett.* **20**, 413 (1973).
(29) I. Fujita and H. Kobayashi, *Inorg. Chem.*, **12**, 2758 (1973).
(30) W. H. Halper, Ph.D. Dissertation, North Carolina State University, 1973, p 12.
(31) L. F. Fieser, "Experiments in Organic Chemistry", D. C. Heath, Boston, Mass., 1957, pp 285–289.
(32) G. A. Heath and R. L. Martin, *Chem. Commun.*, 951 (1969).
(33) G. A. Heath and R. L. Martin, *Aust. J. Chem.*, **24**, 2061 (1957).
(34) K. Bechgaard, V. D. Parker, and C. T. Pedersen, *J. Am. Chem. Soc.*, **95**, 4373 (1973).
(35) C. A. Parker and W. T. Rees, *Analyst*, **85**, 587 (1960).
(36) H. V. Drushel, A. L. Sommers, and R. C. Cox, *Anal. Chem.*, **35**, 2166 (1963).
(37) W. H. Melhuish, *J. Opt. Soc. Am.*, **54**, 183 (1964).
(38) A. J. Barr, J. H. Goodnight, J. P. Sall, and J. T. Helwig, "A User's Guide to SAS 76", Sparks Press, Raleigh, N.C., 1976, pp 193–199.
(39) C. A. Parker, "Photoluminescence of Solutions", Elsevier, Amsterdam, 1968, p 438.
(40) A. Haber and R. P. Runyon, "General Statistics", Addison-Wesley, Reading, Mass., 1971, pp 181–218.
(41) T. J. Durnick and A. H. Kalantar, *J. Chem. Phys.*, **66**, 1914 (1977).
(42) J. R. Lombardi, J. W. Reynolds, and A. C. Albrecht, *J. Chem. Phys.*, **40**, 1148 (1964).
(43) J. N. Demas and G. A. Crosby, *Anal. Chem.*, **42**, 1010 (1970).
(44) G. A. van Salis and H. Labbert, *J. Phys. Chem.*, **72**, 752 (1968).
(45) P. F. Jones and S. Siegel in "Molecular Luminescence", E. C. Lim, Ed., W. A. Benjamin, New York, 1969, p 15.
(46) S. Kawanishi, A. Yokoyama, and H. Tanaka, *Chem. Pharm. Bull.*, **21**, 2653 (1973).
(47) T. J. Chuang and K. B. Eisenthal, *J. Chem. Phys.*, **57**, 5094 (1972).
(48) R. Beckett and B. F. Hoskins, *Inorg. Nucl. Chem. Lett.*, **8**, 683 (1972).
(49) W. C. Galley and R. M. Purkey, *Proc. Natl. Acad. Sci. U.S.A.*, **65**, 823 (1970).
(50) F. Castelli and L. S. Forster, *J. Am. Chem. Soc.*, **95**, 7223 (1973).
(51) F. Castelli and L. S. Forster, *J. Am. Chem. Soc.*, **97**, 6307 (1975).
(52) A. R. Henderson and R. L. Martin, *Aust. J. Chem.*, **25**, 257 (1972).
(53) A. B. P. Lever, "Inorganic Electronic Spectroscopy", Elsevier, Amsterdam, 1968, p 224.
(54) C. K. Jorgensen, "Absorption Spectra and Chemical Bonding in Complexes", Pergamon Press, Oxford, 1962, p 146.
(55) A. M. Bond, G. A. Heath, and R. L. Martin, *J. Electrochem. Soc.*, **117**, 1362 (1970).
(56) A. M. Bond, G. A. Heath, and R. L. Martin, *Inorg. Chem.*, **10**, 2026 (1971).
(57) T. Ohno and S. Kato, *Bull. Chem. Soc. Jpn.*, **47**, 1901 (1974).
(58) J. Wei and C. D. Prater, *Adv. Catal.*, **13**, 204 (1962).
(59) G. Gliemann and H. Yersin, *Ber. Bunsenges. Phys. Chem.*, **75**, 1257 (1971).
(60) F. Castelli and L. S. Forster, *J. Am. Chem. Soc.*, **97**, 6306 (1975).
(61) The Hamamatsu R955 photomultiplier tube used for detection weights light emitted from the blue edge of the emission spectrum most heavily.

Synthesis and Cyclization Reactions of Alkynyl(η^5-cyclopentadienyltricarbonylmolybdenum and -tungsten) Complexes

Patricia L. Watson[1] and Robert G. Bergman*[2]

Contribution from the Division of Chemistry and Chemical Engineering, California Institute of Technology, Pasadena, California 91125, and the Department of Chemistry, University of California, Berkeley, California 94720.

Received August 30, 1978

Abstract: Cyclization of the organometallic complexes $CH_3C{\equiv}C(CH_2)_nM(C_5H_5)(CO)_3$ (n = 3, 4, 5; I, M = Mo; II, M = W) occurred under mild conditions to give cyclized products $M(C_5H_5)(CO)_2[C(CH_3){=}C(O)(CH_2)_n]$ (III, M = Mo; IV, M = W) derived from intramolecular insertion of the acetylenic function into a metal–acyl bond. Yields of III were high (>70%) for n = 3, moderate (~50%) for n = 4, and lower (<15%) for n = 5. No other isomers or products of insertion into metal–alkyl bonds were observed. Cleavage of the organic ligand from III (n = 4) under CO with CF_3COOH gave 2-ethylidenecyclohexanone and $CF_3CO_2Mo(C_5H_5)(CO)_3$ in >90% yield. Hydrogenation of III (n = 4) gave 2-ethylcyclohexanone and $[Mo(C_5H_5)(CO)_2]_2$ in >90% yield. Protonation of $CH_3C{\equiv}C(CH_2)_4W(C_5H_5)(CO)_3$ gave the bis acetylene complex, $W(C_5H_5)(CO)_2(2\text{-heptyne})_2^+$.

Introduction

Cyclization of acyclic ω-functionalized acetylenes A has been mediated by a number of metal reagents, yielding several kinds of products. Examples include RCuLi reagents[3a] (effective primarily for R = phenyl and n = 3, 4), which give products of type B and C, $PdI_2/CO/PBu_3$[3b,c] for X = OH, which give the compounds D, and $Ni(CO)_4/OR'^-$ [3d] for X = halide, which yield products of type E and F. Variation in ob-

0002-7863/79/1501-2055$01.00/0